(Received 2 March 2026, Accepted 3 April 2026, Scheduled 8 May 2026)

Design and Optimization of Four-Coil Magnetic Coupled Resonant Wireless Power Transfer

Sylcolin Rakotonandrasana[1], Bilal A. Khawaja[1], Habachi Bilal[2], Jeannot Velontsoa[3,4], Leonide Tongazara[4], Sébastien Lalléchère[5,*], Glauco Fontgalland[6], Fayu Wan[7], and Blaise Ravelo[7]

[1]*Faculty of Engineering, Department of Electrical Engineering, Islamic University of Madinah P. O. BOX 170, Madinah 41411, Saudi Arabia*
[2]*Laboratory of Innovative Technologies (LTI) UR 3899, University of Picardie Jules Verne (UPJV), 80000 Amiens, France*
[3]*Institut Supérieur de Technologie D'Antsiranana (ISTD), 201 Antsiranana, Madagascar*
[4]*University of Antsiranana, 201 Antsiranana, Madagascar*
[5]*Association Française de Science des Systèmes (AFSCET), 92260 Fontenay-aux-Roses, France*
[6]*Brenton School of Engineering, University of Mount Union, Alliance, OH 44601, USA*
[7]*School of Electronic & Information Engineering, NUIST, Nanjing 210044, Jiangsu, China*

ABSTRACT: Magnetic Coupled Resonant (MCR) Wireless Power Transfer (WPT) is typically used for electrical charging, offering high tolerance to misalignment and wider transmission range. However, MCR-WPT is assumed to be a two-port circuit, including transmitter (Tx) and receiver (Rx), and exhibits lower efficiency than conventional inductive power transfer. Various studies have been proposed to increase the 4-coil MCR-WPT efficiency, but further challenges remain due to the turn technology complexity. A relevant and simple design solution is developed in the present paper that enables the optimization of Power Transfer Efficiency (PTE) by minimizing implementation cost. To achieve that goal, the transfer- and resonator-distances, TD and RD, respectively, were optimized through theory, both circuit and 3-D electromagnetic (EM) simulations via 3-D modeling and experimentation. The validation PTE results obtained from analytic calculation, simulation, and experimentation affirm that the maximum efficiencies of 94.10, 90.15%, and 69.35% were obtained at optimal positions around $RD = 7.5$ mm and $TD = 100$ mm, respectively. The slight difference of the obtained PTE among theory and simulation with experiment is due to the setup instrument imperfection. The performed study is useful for WPT charging systems, such as electronic sensors, wearable devices, and communication systems.

1. INTRODUCTION

Nowadays, Wireless Power Transfer (WPT) systems are among the most widely used for charging electronic, portable [1–3], and medical devices [4]. By analyzing power intensity, WPT systems are categorized into two distinct groups as very low-voltage (LV) systems, referenced in [5–7], and high-voltage (HV) systems, discussed in [8–11]. In the category of low-voltage WPT systems, Near-Field Communication (NFC) [5] is a practical, everyday technology due to its integration into wearable objects in both passive and active modes. NFC WPT is more convenient to operate in Radio Frequency (RF), particularly in the megahertz (MHz) range [6]. The NFC WPT is integrated in portable devices, such as smartphone applications, and it can be designed to avoid electromagnetic interference (EMI) by using a metal-cover technique [7]. In the field of HV systems, WPT is increasingly used to charge electric vehicles [8–11], where the position between the source and load is a critical point and remains a focus of research in electrical and electronic engineering.

From a perspective of a topological circuit, there are two primary types of WPT systems: inductive [5, 7, 10, 11] and capacitive [12], as detailed in [13]. The Inductive Power Transfer (IPT) system enables energy transmission with free-positioning of the electric battery [14, 15]. The IPT system works with electromagnetic (EM) mutual coupling between the energy transmitter (Tx) and receiver (Rx). The IPT is now emerging as a modern trend in electric transportation applications [16]. The HV IPTs cover a wide range of applications, such as underwater engines [17, 18] and unmanned aerial vehicle (UAV) charging platforms [19]. The practical use of charging systems in omnidirectional and free-positioning applications has led to the study of the design and analysis of the constituent coils for WPTs [20, 21]. The definition of electrical, EM, and mechanical parameters that affect the efficiency of WPTs remains a challenge for design and manufacturing engineers. For example, an estimation method of mutual inductance in a WPT system was formulated [22]. A relevant study enabling the choice of the configuration [23, 24] and the modeling of the electric circuit, including the equivalent impedance [25] for WPT applications, is necessary. In addition to the configuration, the IPT circuit loss must be taken into account [26, 27], including the skin effect, which can be particularly significant at RF ranges [28]. Specific attention must be focused on how to maximize the Power Transfer Efficiency (PTE) of WPT in function of its constituting parameters [29, 30]. Therefore, methods were pro-

* Corresponding author: Sébastien Lalléchère (sebastien.lallechere@protonmail.com).

posed to model and optimize the topology of IPTs [31, 32] and also include the magnetic shielding [33].

To increase the PTE, several design approaches have been explored by research designers. Nevertheless, so far, many of the IPT design studies remain an open research topic. For example, so far, the WPT implementation with multiple coils [34–37], including the influence of Magnetic Coupled Resonant (MCR) EM energy transfer distance [38] between Tx and Rx, is a hot topic. Different enhancement techniques were designed to optimize the PTE [39–41]. Simulation methods were also proposed by using designers operating under EM full-wave solvers [4, 42]. For the case of four-coil-based WPT, further study is expected to optimize the PTE. The present research work investigates the design of optimal 4-coil-based MCR-IPT, including EM full-wave simulations and measurement versus the transfer distance (TD) between transmitter (Tx) and receiver (Rx) coils, combined with resonator distance (RD) between Tx and drive (Dx) coils or Rx and load (Lx) coils. To do this, the paper is organized as follows. Section 2 covers the literature review, including the topological study and specifications of the 4-coil MCR-WPT structure. Section 3 explores the design theory and modeling, combined with the optimization approach for the 4-coil MCR-WPT PTE. Section 4 focuses on the proof-of-concept (PoC) design of the 4-coil MCR-WPT after selecting parameters optimized for the physical distance. Section 5 validates the PTE study through S-parameters obtained from full-wave simulations using a commercial tool, as well as the experimental testing of a prototype with a vector network analyzer (VNA). Finally, Section 6 presents the conclusion.

2. LITERATURE REVIEW ON COUPLED-COIL STRUCTURE OPTIMIZATION

The literature review, specifications, design, and optimization approach of the 4-coil MCR-WPT topology are introduced in this section.

2.1. Preliminary on the 4-MCR-WPT Coil Design

The conductor coil constituting the Tx and Rx structure is the most crucial component of a WPT. Understanding coils' operating principle related to Tx-Rx coupling coefficient k requires basic knowledge, such as Faraday's law, eddy current, skin- and proximity-effect. The resistivity of the conductor wire increases due to the reduction of the effective cross-sectional area available for electron flow, which is the consequence of skin and proximity effects [28]. Resonance at an appropriate frequency can be exploited to improve the EM PTE in the 4-coil MCR-WPT as illustrated in Fig. 1.

Among existing WPT studies, few were focused relatively on each element positioning. The system in Fig. 1 is supplied by input voltage v_{in} through drive coil Dx and loaded by resistor R_l producing output v_{out} across the load coil Lx. The 4-coil WPT topology includes capacitors C_t and C_r acting as Tx and Rx compensators, respectively, with inner diameter D_{in} and outer diameter D_{out}. For a 4-coil MCR-WPT system, the operating frequency is pushed to MHz to achieve a more compact coil design [6]. To be specific, for safety reasons, Industrial Scientific Medical (ISM) frequencies, such as 6.78, 13.56, and 21.12 MHz, are proposed [43]. At those frequencies, skin and proximity effects become significant in most conductive materials. Furthermore, switching losses can be reduced by using wide-bandgap semiconductors, such as Silicon Carbide (SiC) and Gallium Nitride (GaN) [44, 45]. An important advantage of 4-coil MCR-WPT systems is the ability to increase the transfer distance (TD) between Tx and Rx coils while maintaining good tolerance to misalignment. However, the WPT system's power transfer capability is strongly affected by variations in TD [6]. This work develops an efficiency optimization approach without increasing system cost. To achieve this, attention is given to coil impedance as well as to the distances between Dx and Tx, and between Lx and Rx resonators, referred to as RD. Before presenting the analytical investigation of the 4-coil MCR-WPT circuit, a topological optimization is provided in the following subsection.

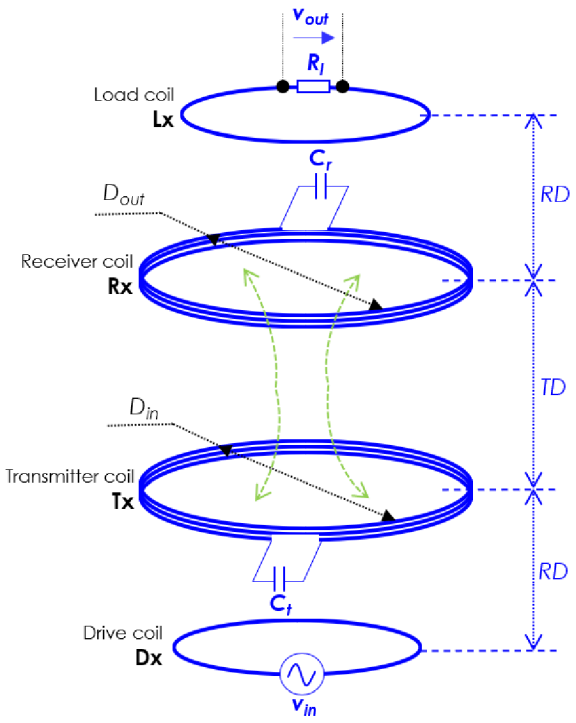

FIGURE 1. Topology of 4-coil MCR-WPT.

2.2. MCR-WPT Topological Optimization

The most effective way to improve WPT efficiency is to tune the value of k. This parameter can be evaluated theoretically, through simulations, and experimentally. Additionally, the impact of practical environmental factors can be characterized experimentally by minimizing imperfections and undesirable EMI. For instance, Finite Element Analysis (FEA) simulation in a 3D design enables optimization of k for WPT by combining a DD-type coil with a solenoid-type coil [9]. However, adding a solenoid coil to the design increases the length and weight, leading to higher costs. So far, many pad configurations have been found, but the 4-coil MCR-WPT illustrated in Fig. 1 stands out from the conventional coil type with its high

TABLE 1. Review of four-coils design, optimization techniques, and results

Coil characteristics	Frequency	Optimization parameter	Ratio	η_{max}
Circular $D_{in} = 10$ cm; $TD = 4$ cm [42]	14.17 MHz	Resonance frequency	0.4	72.5%
Square width $W = 5$ cm; $TD = 5$ cm [27]	13.56 MHz	Minimize material losses	1	66%
Circular $D_{in} = 10$ cm; $TD = 3$–15 cm [38]	20 MHz	TD with multiple Secondary (Rx, Lx)	0.3	$< 60\%$
Square $W = 80$ cm; $TD = 20$ cm [8]	90 kHz	Asymmetric four coil	0.25	96.56%
Circular $D_{in} = 50$ cm; $TD = 30$ cm [39]	100 kHz	L-matching Network	0.6	66.8%
Circular $D_{out} = 30$ cm; $TD = 25$ cm [40]	13.56 MHz	TD with multiple D_{out} for Lx and Dx	0.83	93.3%
Circular $D_{out} = 60$ cm; $TD = 35$ cm [23]	≈ 7 MHz	Lx and Dx position with TD	0.58	82.5%
Circular $D_{out} = 82$ cm; $TD = 3$ cm [4]	9.1 MHz	D_{out} for Lx and Tx	0.035	33%
Helical $D_{in} = 15$ cm; $TD = 11.67$ cm [26]	589 kHz	Resistive loss in Tx and Rx	0.78	72%
Pentagon $W = 20$ cm; $TD = 12$ cm [41]	13.56 MHz	k_{12} and TD or k_{34} and TD	0.6	35%

tolerance to misalignment, long range of TD capability [10]. Regarding the circular 4-coils, EM simulations allow for reaching a PTE $\eta = 72.5\%$ at the resonance frequency of 14.17 MHz [42]. However, the optimization work was only focused on the frequency. Another attempt proposes a printed square shape of 4-coil WPT for compact WPT from different materials to analyze the material losses, and they achieved $\eta = 66\%$ with 57% of the losses being resistive and 37% ohmic [29]. Additionally, the simulation of multiple Rx coils of 4-coil MCR enables obtaining maximum PTE below 60% [38]. Moreover, in [48], parameters like N, s, i, D_{out}, and D_{in} are taken as variables to optimize power output and transfer efficiency; however, this work concerns a two-coil topology, and the application for 4-coil structure is missing. Further optimization approaches are discussed in the following subsections.

2.3. Optimization by Distance Adjustment

This type of optimization involves mechanically adjusting RD and TD. However, this technique indirectly affects the WPT circuit impedance. As an example of distance adjustment, the resonator position is rearranged through a combination of inside and outside placements. It was found that PTE trends similarly. For example, as reported in [23], the experimental work gave a maximum efficiency of 82.5% with $TD = 35$ cm and $D_{out} = 60$ cm. Another method to address the spatial variation between turn-through simulation and experimentation was proposed to improve PTE by 10% and reduce sensitivity to angular and lateral misalignment [21]. In this research, PTE optimization is elaborated by varying RD while holding TD fixed to optimize PTE, and vice versa. Additionally, to follow the standard proposed for the ISM band [6], the AirFuel Alliance frequency, specifically 6.78 MHz, is fixed to be reached as the resonance frequency.

2.4. Optimization by Impedance Matching

In addition to the compensator circuit that regulates frequency to resonance, impedance matching is required during load variations, for example, in a battery-charging application. As an example, to optimize PTE, a fast-tracking optimum efficiency was proposed to first estimate the input impedance according to TD, then adjust the load with an L-type matching network [39]. Despite being able to improve PTE by roughly 70% with a $TD = 25$ cm, this method requires adding and adjusting the inductor, capacitor bank, and switches. That approach would complicate the design to control and operate. Additionally, the L-Type network is not the only method to optimize MCR-WPT; there are T-Type and π-Type networks as well, and they perform better than L-Type [6]. In addition to that, for comparison purposes, of several studies concerning four-coils, Table 1 is proposed as a survey to list specifically the coil parameters used for optimization, the maximum of η obtained, the frequency targeted, and the ratio:

$$a_{in,out} = TD/D_{in,out} \tag{1}$$

to estimate the performance of the coil with respect to its size. After the survey, it can be concluded that the ratio is mostly ≤ 1, which can be interpreted as that the coil's diameter is bigger than TD. Furthermore, very few researchers use the kHz range, but it shows high efficiency similar to that in the MHz range.

However, the optimization technique is diversified with the repetition of TD analysis. The approach introduced in [41] attracts our attention by optimizing k and TD. However, in this search work, we want to improve the ratio a_{in} or a_{out} and include the 3-D model analysis of the four coils in an EM commercial tool software. The following section describes the 4-MCR-WPT theoretical design with the considered optimization technique.

3. THEORETICAL DESIGN OF 4-MCR-WPT VIA DX-TX, TX-RX AND RX-LX DISTANCE OPTIMIZATION

The theoretical design of 4-coil MCR-WPT, including the Dx-Tx, Tx-Rx, and Rx-Lx distance optimization, is elaborated in the present section.

3.1. Design Methodology

The design methodology of the four-coil MCR-WPT system is organized into six steps as follows:

TABLE 2. Mathematical expression of circular coil inductance.

Coil shape	Descriptions	Inductance	
Circle loop [5]	Single loop wire: $N = 1$	$L = N^2\mu_0\mu_r D_{in}[\ln(8D_{in}/s) - 7/4]/2$	(2)
Spiral circular [46, 47]	$D_{avg} = (D_{in} + D_{out})/2$, $p = (D_{out} - D_{in})/(2D_{avg})$, $C_1 = 1, C_2 = 2.46$, $C_3 = 0$ and $C_4 = 0.2$ for Equation (3)	$L = N^2\mu_0\mu_r \frac{D_{avg}C_1}{2}\left[\ln\left(\frac{C_2}{p}\right) + C_3 p + C_4 p^2\right]$	(3)

- **Step 1 — Mathematical modelling of coils**: This step consists of the analytical modelling of the MCR-WPT S-parameters, considered as a two-port network, focusing on return- (S_{11} and S_{22}) and insertion- ($S_{12} = S_{21}$) losses. The model includes the computation of lumped elements, such as self-capacitance and self-inductance, while accounting for skin effect to estimate the AC internal resistance of the coils.
- **Step 2 — Equivalent circuit simulation**: The S-parameter simulation must include compensation networks represented by series capacitors C_r and C_t connected to the Tx and Rx coils using optimized values.
- **Step 3 — PoC design and EM simulation**: A 3D design and simulation of the 4-coil MCR-WPT system are required to account for realistic EM effects. A commercial software tool such as Computer Simulation Technology (CST) Studio Suite can be used to perform full-wave simulations. The influence of Tx and Rx compensators can be evaluated by varying capacitor values.
- **Step 4 — Optimization process**: The optimization of the 4-coil MCR-WPT system involves both electrical and geometrical parameters, including wire diameter s, spacing i, length l, TD, RD, and number of turns N. The originality of the proposed approach lies in the combination of analytical and simulation-based optimization.
- **Step 5 — Prototyping**: An experimental demonstrator is fabricated based on the optimized PoC design obtained in the previous step.
- **Step 6 — Experimentation and analysis**: The PTE evaluation is carried out by comparing simulation results with experimental measurements to validate the proposed design and optimization methodology.

The analytical modeling approach is detailed in the next subsection.

3.2. PTE Analytical Modeling from *S*-Parameters

The analytical modeling initially centers on the governing equations of the constituent coils. The equivalent component values of the coil can be adjusted according to the physical dimensions as D_{in} and D_{out}, and also the constituting material properties, including the permeability $\mu_0\mu_r$. Table 2 summarizes the analytical relations between the material properties and physical dimensions of coil inductance [5, 46].

In addition to its inductance, a coil has two more important parameters, the resistance at a given frequency R_{ac} and the self-capacitance C_{self}. R_{ac} is proportional to f at which the coils operate, due to the skin effect and proximity effect [28]. To model a coil, the parameters to compute are the DC resistance R_{dc}, which is proportional to the coil length and described as:

$$R_{dc} = 4\rho l/(\pi s^2) \tag{4}$$

where ρ is the conductor resistivity (copper wire 1.68×10^{-8} [$\Omega \cdot$ m] at 20°C); l is the coil total length; and s is the wire diameter. Then, the AC resistance at the resonance frequency, which is fixed and chosen carefully to meet the ISO standard for safety reasons, is caused by the EM exposure as stated in [43]:

$$\delta = \sqrt{\rho/(\pi f \mu)} \tag{5}$$

$$R_{skin} = R_{dc}\left(1 + s/\delta + 3\delta/(4s)\right)/4 \tag{6}$$

$$R_{prox} = R_{dc}\pi^2 s^2 H^2 \left(s/\delta - 1\right)/(2I_0^2) \tag{7}$$

$$R_{ac} = R_{skin} + R_{prox} \tag{8}$$

To minimize the frequency influence that causes the skin effect resistance (R_{skin}) and proximity effect resistance (R_{prox}), the Litz wire is used. However, it would not be recommended for the frequency above 1 MHz [49]. After that, to compute the coil self-capacitance of the wire that has N turns, the thickness of the coating material and its permittivity ε_r [50] were considered. However, the ISM standard suggests the frequency of 6.78 MHz to avoid damaging living tissue and to obtain the coil that resonates at this frequency, a compensation network made of a capacitor with value C_{ss}, mounted in series, is required. Additionally, C_{self} is the neglected compared to C_{ss}. Therefore, the values of L and C_{ss} will be used to find the resonance frequency f_0 of the coil and combined with the value of R_{ac} to predict η as described by the following equations [5]:

$$C_{ss} = 1/\left[(2\pi f_0)^2 L\right] \tag{9}$$

$$Q_i = \omega L_i/R_i \tag{10}$$

$$M_{ij} = 0.5\pi N_i N_j \mu_0\mu_r r_i^2 r_j^2/\left[d_{ij}^2 + (r_i + r_j)^2\right]^{3/2} \tag{11}$$

$$k_{ij} = M_{ij}/\sqrt{L_i L_j} \tag{12}$$

To avoid repeating (10), (11), and (12) for each coil Tx, Rx, Dx, and Lx, annotations i and j are parameters related to coil$_i$ and coil$_j$. For example, k_{TR} means the coupling factor between Tx and Rx; M_{DT} is the mutual inductance between Dx and Tx; d_{RL} is the distance between Rx and Lx; and r_D is the Dx radius. Moreover, because of the symmetricity of the design, $k_{DT} = k_{RL} = k_{lc}$, $k_{RT} = k_{TR} = k_c$, $Q_R = Q_T = Q_c$, and $Q_L = Q_D = Q_{lc}$. Finally, η is the square of insertion loss absolute value $|S_{21}|$. In other words, η can be expressed in function of coupling factors k_c and k_{lc} and, quality factors Q_c and Q_{lc} [38, 40, 42]:

$$\eta = |S_{21}|^2 = 4\left|k_{lc}^2 k_c Q_{lc} Q_c^2 / \left[\left(1 + k_{lc}^2 Q_{lc} Q_c\right)^2 + 1 + k_c^2 Q_c^2\right]\right|^2 \tag{13}$$

$\mu_0 = 4\pi \times 10^{-7}$ H/m is the free space permeability; μ_r is the conductor material relative permeability; l is the coil length; and d_{ij} is the air gap distance between two coils (TD or RD). In addition, the author in [51] experimentally investigated the impact of system parameters on WPT PTE, emphasizing the role of coupling and losses in practical implementations. Thus, to validate the 4-MCR-WPT design and optimized method, a PoC was drawn with parameters assigned in the commercial tool as discussed in the next section.

4. PROOF-OF-CONCEPT (POC) DESIGN INTEGRATING OPTIMIZED PARAMETERS

After the numerical witness on the coil positioning optimization from the previous theoretical approach, the design of MCR-WPT PoC is described in the present section. The 4-MCR-WPT validation study is carried out at the frequency $f_0 = 6.78$ MHz.

4.1. PTE Analytical Optimization for PoC Design

From Equation (11), it can be observed that the distance d is inversely proportional to mutual M, but the latter is proportional to k according to (13). Therefore, increasing d will decrease k, and that claim is proved in [41]. Fig. 2 indicates that for each value of k_c, there is an optimal k_{lc} that yields maximum efficiency. Table 3 lists the characteristics of the employed coil after calculations and the optimized value of PTE.

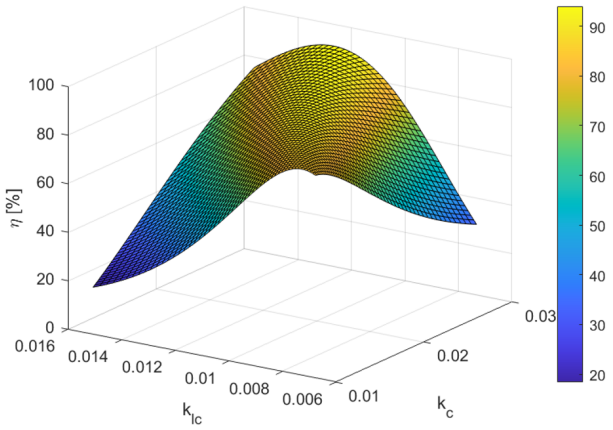

FIGURE 2. PTE variation illustrating the optimization of pair (k_c, k_{lc}).

TABLE 3. Coil parameters after analytical operations.

Coil parameters	Tx and Rx (c)	Dx and Lx (lc)
Coil diameter	$D_{out} = 13$ cm	$D_{in} = 10$ cm
Conductor diameter	$s = 1$ mm	
Number of turns	$N = 10$	$N = 1$
Inductance	$L_c = 21.25$ µH	$L_{lc} = 310$ nH
Mutual inductance	$M_c = 610$ nH	$M_{lc} = 31.29$ nH
Length	$l_c = 3.6128$ m	$l_{lc} = 314$ mm
$R_{ac}(f_0)$	$R_c = 790.85$ mΩ	$R_{lc} = 68.8$ mΩ
SS capacitor	$C_c = 25.93$ pF	$C_{lc} = 1.78$ nF
Skin depth (f_0)	$\delta = 25.05$ µm	
Maximum efficiency	$\eta = 94.1\%$	

In other word, there is an optimal RD (resp. TD) for each specific value of TD (resp. RD). An MCR-WPT PoC was designed to verify the relevance of the optimization approach. The next subsection describes the PoC designed with the CST tool.

4.2. PoC CST Design

Figure 3 shows the 3-D design of the 4-coil MCR-WPT PoC, including the Tx and Rx lumped ports representing the C_t and C_r compensators, whose values were calculated from Equation (9).

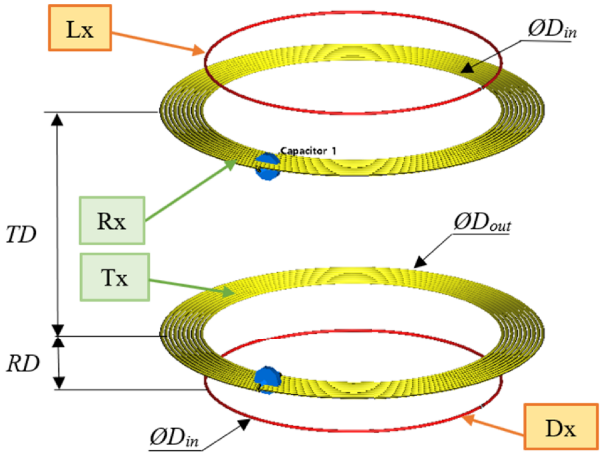

FIGURE 3. PoC of 4-coil MCR-WPT CST design.

In this 3-D CST design, we have four coils constituted by two resonator coils for Tx connected to the feeding source connected to drive coil Dx, and Rx associated with the load coil Lx. Many software programs can be used to compute coil performance, such as ANSYS HFSS and COMSOL Multiphysics. The choice to design the PoC by using the commercial tool CST was to compute the S-parameters of the coupled coil and the possibility to compare that result using a VNA tester on the prototype. The conductor material used is copper, and the wire diameter is set to $s = 1$ mm. Then, the resonator coils Rx, Tx, Dx, and Lx diameters are fixed to D_{in} =100 mm and $D_{out} = 115$ mm. The coupling physical distances TD and

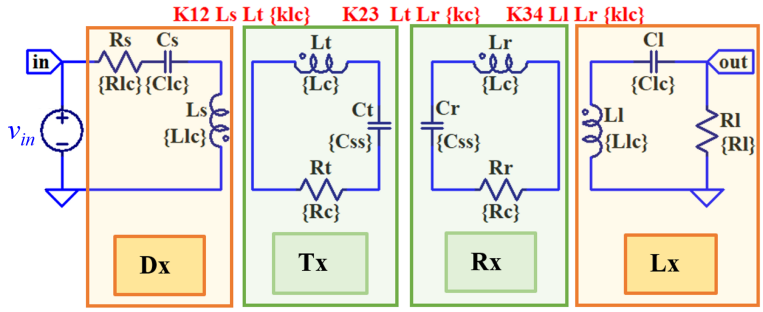

FIGURE 4. 4-coil MCR-WPT electrical circuit equivalent.

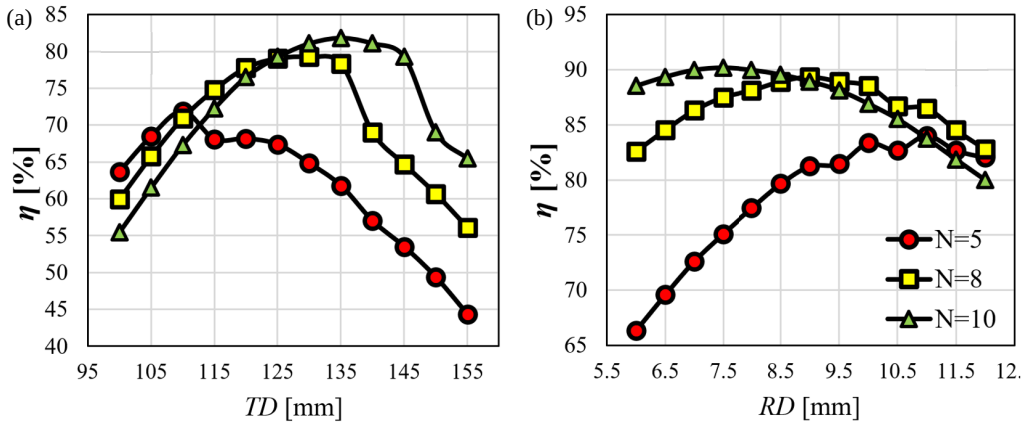

FIGURE 5. PTE optimization when (a) $RD = 17$ mm and (b) $TD = 100$ mm.

RD are gradually changed to enhance η. Fig. 4 schematizes the electrical circuit equivalent to the PoC of 4-coil MCR-WPT, which includes the models of R_i, L_i, and C_i constituting components.

The input parameters of the simulation were set to match the experimental coils as closely as possible. The maximum number of turns N is set to be 10 because a higher turn number would be time-consuming, and the available resource limits us to 10, then decreased to 8, and finally to 5, to see its effect on the efficiency. The prototyping and validation results from simulation and measurement are discussed in the next section.

5. OPTIMIZED 4-COIL MCR-WPT PROTOTYPING, EXPERIMENTATION AND DISCUSSION ON VALIDATION RESULTS

Using the previous design and optimization methodology, the analysis of 4-coil MCR-WPT prototyping and validation results is the main focus of the present section.

5.1. Simulation Results

After running the frequency domain solver (FDS), one obtains the S-parameter results. Then, the PTEs were derived by Equation (13). The obtained abacuses for two cases, $RD = 17$ mm fixed and optimized TD varied from 95 mm to 155 mm, plotted in a line chart in Fig. 5(a). Similarly, the PTEs for optimized RD from 5.5 mm to 12 mm at a fixed $TD = 100$ mm are shown in Fig. 5(b). We can remark on two aspects from the optimization. On one hand, as indicated in Table 4, from Fig. 5(a) (resp. 5(b)), when $RD = 17$ mm (resp. $TD = 100$ mm) is fixed, $\eta_{\max}$ is obtained when varying N and TD (resp. RD). How to optimize distances by adjusting RD and TD to reach higher efficiency is clear from the demonstration graphics illustrated by Fig. 5.

TABLE 4. Maximal PTE versus pair (N, TD).

Fig.	5(a)			5(b)		
RD	17 mm			11 mm	9 mm	7.5 mm
TD	110 mm	130 mm	135 mm	100 mm		
N	5	8	10	5	8	10
$\eta_{\max}$	71.88%	79.25%	81.85%	84.02%	89.33%	90.15%

On the other hand, concerning S_{11} and S_{21}, at the optimal efficiency, which is the highest magnitude of S_{21}, the reflection coefficient S_{11} reaches the lowest one. It means that the maximum power is transmitted from Tx to Rx. For example, three cases where $RD = \{7.5\,\text{mm}, 9\,\text{mm}, 11\,\text{mm}\}$ with $TD = 100$ mm show where S_{21} reached its peak when $N = \{10, 8, \text{and } 5\}$, respectively. Therefore, it can be emphasized from the S-parameter results of the simulation that higher N improves the efficiency, but compared to lower TD, wider TD is less efficient, which is confirmed by the results found in [10, 13]. Furthermore, for a fixed TD, RD can be adjusted to enhance η and the maximum transmitted power.

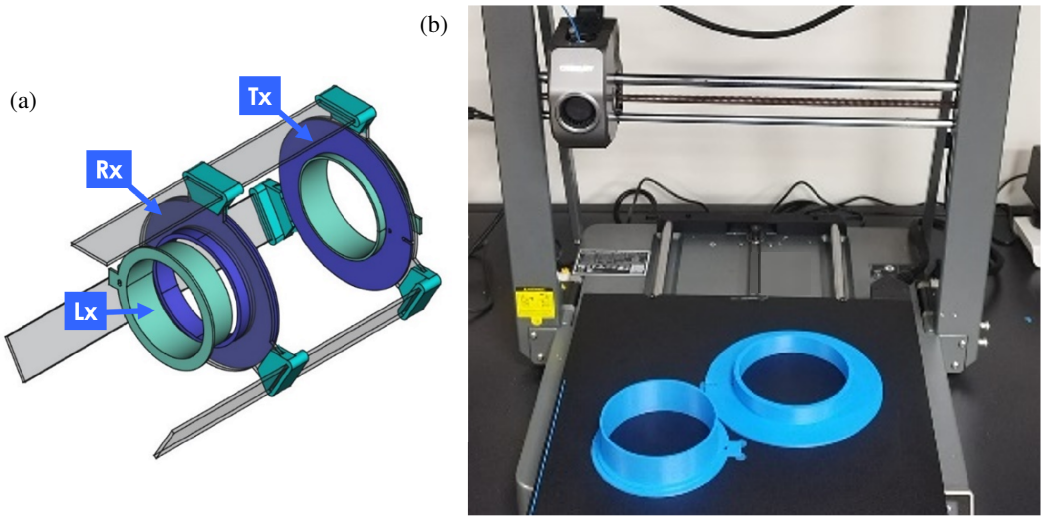

FIGURE 6. 4-coil MCR-WPT (a) CAD design and (b) 3-D printing manufacturing.

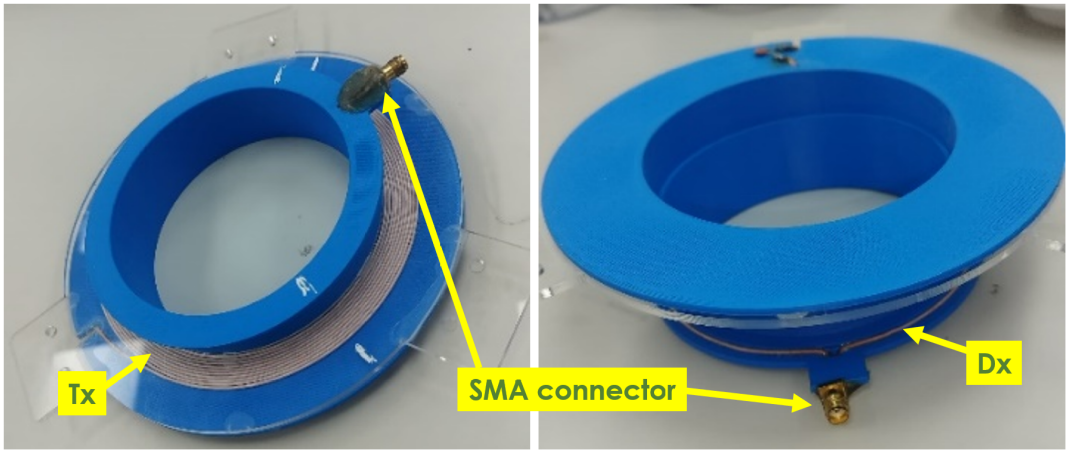

FIGURE 7. Photos of Tx and Dx MCR-WPT prototypes.

This optimization enables the choice of relevant specifications of the 4-coil MCR-WPT PoC. Then, according to the fabrication facilities, the prototype was manufactured. The obtained validation test results are treated in the following subsection.

5.2. Prototyping and Experiment Test Setup

To prototype a WPT demonstrator, a 3-D virtual structure was designed with the commercial tool FreeCAD software. The corresponding 3-D perspective highlighting the assembly parts of the 4-coil MCR-WPT virtual prototype is presented in Fig. 6(a).

The design files from FreeCAD were exported to the 3-D printer to manufacture the real prototype. One feature of the experimental test was a support designed to facilitate the TD and RD adjustment. However, the turn number, wire diameter, and space were fixed to $N = 10$, $s = 1\,\text{mm}$, and $i = 0.5\,\text{mm}$, respectively. Fig. 6(b) shows a photograph of the 3D printer employed during the prototype manufacturing process. The Tx and Rx real capacitors having nominal values $C_{tn} = C_{rn} = 27\,\text{pF}$ and the Dx capacitor $1.8\,\text{pF}$ were chosen from the E-24 series of existing components available in our laboratory. The photos of the Tx and Dx coils constituting the experimented 4-coil MCR-WPT prototype are displayed in Fig. 7. The synoptic diagram and a photograph of the experimental setup of the fabricated four-coil MCR-WPT prototype are shown in Fig. 8(a) and Fig. 8(b), respectively. During the test, the MCR-WPT device was connected to a VNA using SMA connectors. A Keysight N9916B FieldFox Microwave Analyzer, operating over the 30 kHz–14 GHz frequency range, was used to measure the PTE of the four-coil MCR-WPT prototype.

After performing a standard Short-Open-Load-Thru (SOLT) calibration, the measured S-parameters were recorded in Touchstone format and subsequently converted into PTE values. In addition, measurement uncertainties must be considered when the experimental results are analyzed. These uncertainties arise from several sources, including calibration residual errors of the VNA, connector repeatability, cable

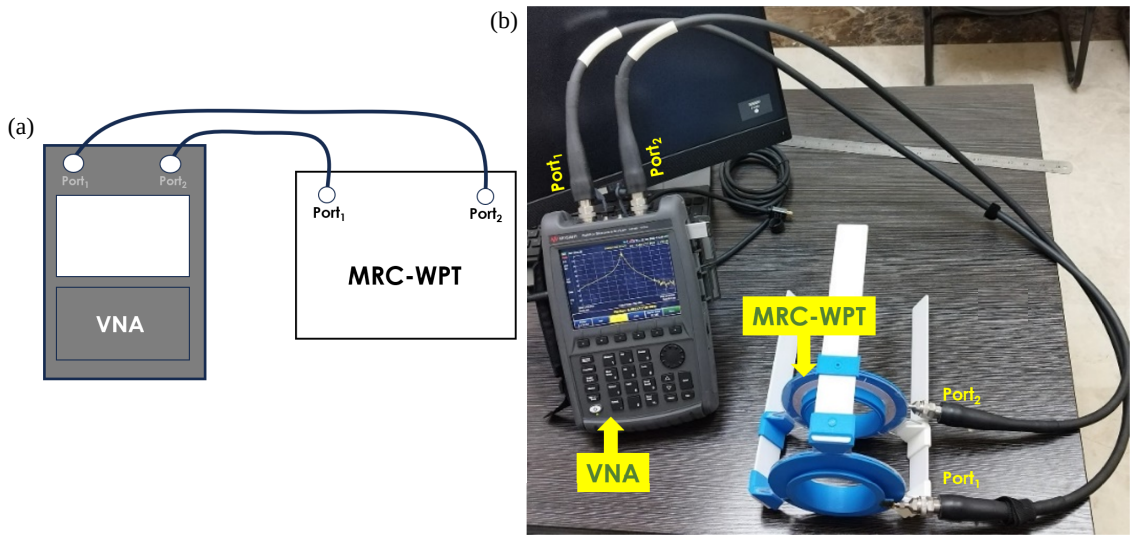

FIGURE 8. (a) Synoptic diagram and (b) photo of experimental setup for the MCR-WPT S-parameter measurement.

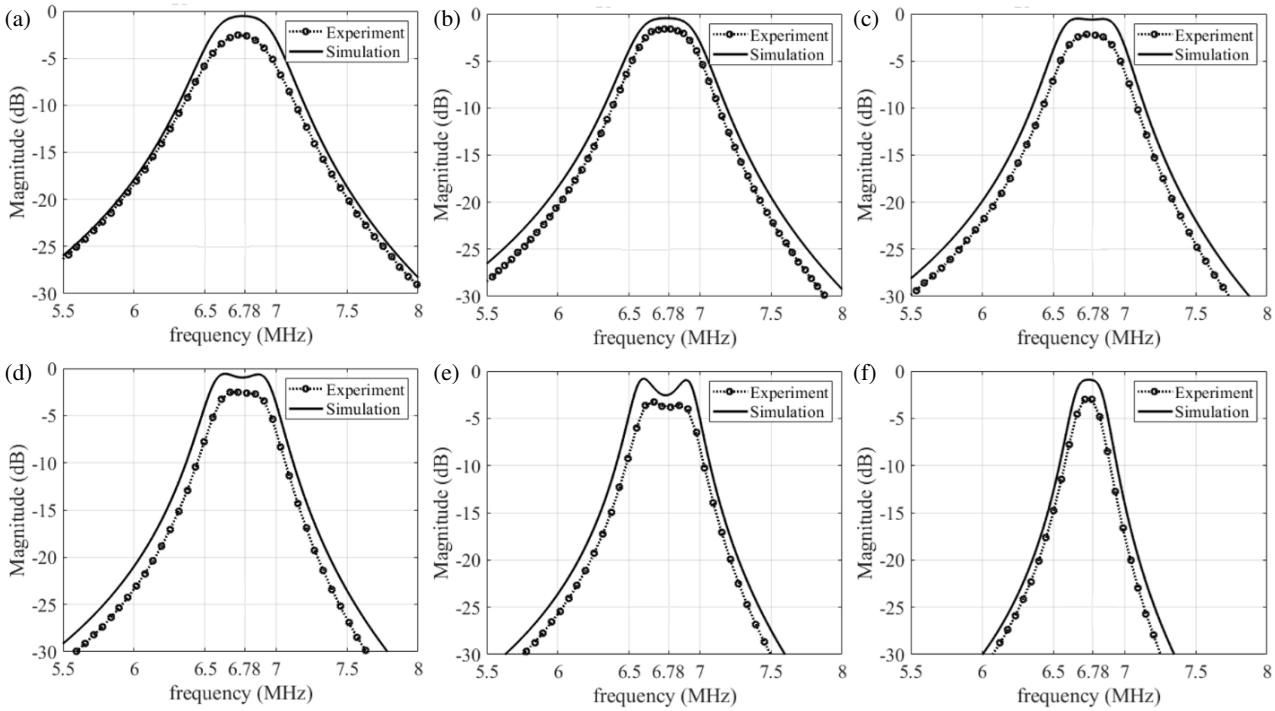

FIGURE 9. Insertion losses results comparison from experiment and simulation: (a) ($TD = 100$ mm, $RD = 6$ mm), (b) ($TD = 100$ mm, $RD = 7.5$ mm), (c) ($TD = 100$ mm, $RD = 10$ mm), (d) ($TD = 100$ mm, $RD = 12$ mm), (e) ($TD = 100$ mm, $RD = 17$ mm) and (f) ($TD = 140$ mm, $RD = 17$ mm).

losses, and environmental variations. The accuracy of the Keysight N9916B analyzer, particularly in the considered frequency range around 6.78 MHz, also contributes to measurement deviations. Moreover, imperfections in the SOLT calibration procedure and mismatch effects at the SMA interfaces can introduce additional uncertainty in the measured S-parameters. These combined factors partly explain the discrepancy observed between simulated and experimental PTE results and should be taken into account when interpreting the performance of the proposed WPT system. The comparison among calculated, simulated, and measured results of the four-coil MCR-WPT prototype is presented in the next subsection.

5.3. Discussion among Calculated, Simulated, and Experimented PTE

The experimentation process consisted of measuring the 4-coil MCR-WPT S-parameters from $f_{\min} = 5.5$ MHz to $f_{\max} =$

TABLE 5. PTE from calculation, simulation, and measurement results.

TD [mm]	RD [mm]	η_{theory} [%]	η_{CST} [%]	η_{exp} [%]
100	6	86.27	88.51	55.40
	7.5	94.10	90.15	69.35
	10	87.84	86.90	60.13
	12	74.83	79.98	54.53
	17	32.18	55.46	41.28
140	17	82.57	81.10	50.53

8 MHz for different values of TD and RD. The series of practical tests were carried out by fixing and increasing one of the distances TD and RD gradually. Two different phases were considered: **(i) Phase 1:** The first phase consisted in setting $TD = 100$ mm and measuring S_{21} for different positions $RD = \{6\,\text{mm}, 7.5\,\text{mm}, 10\,\text{mm}, 12\,\text{mm}, 17\,\text{mm}\}$ and **(ii) Phase 2:** The other phase was performed by fixing $RD = 17$ mm and measuring S_{21} for varied positions $TD = \{100\,\text{mm}, 145\,\text{mm}, 155\,\text{mm}\}$. The insertion losses spanned from f_{min} to f_{max}, which were tested with the VNA and compared with the simulation results from CST. Furthermore, the efficiency (η) was quantified based on the insertion losses with respect to relation (13). Therefore, we obtain the comparative plots of S_{21}, illustrated in Fig. 9. We remark that: (i) Good agreement between simulated and measured insertion losses is observed within the frequency band. (ii) Additionally, S_{21} tends to become narrower for higher TD values, with a similar effect observed for lower RD values. (iii) The family of curves confirms the relevance of the proposed optimization methodology. When a valley or flat region appears at the peak of S_{21}, efficiency can be optimized by either increasing TD or decreasing RD. (iv) The experimental results show lower efficiency than simulations due to parasitic losses in the wires, connection resistances, and the permeability of the plastic support. Moreover, Table 5 presents the PTE values obtained from theoretical analysis, simulation, and experimental measurements. The following points can be noted: The proposed design method for the four-coil MCR-WPT system, which optimizes PTE (η) by adjusting RD and TD, is validated experimentally. For $TD = 100$ mm, η reaches its maximum when $RD = 7.5$ mm. The numerical calculation of η using Equation (13) yields a maximum efficiency of 94.1%. However, CST simulations provide approximately 90.15%, while measurements reach 69.35% for $TD = 100$ mm and $RD = 7.5$ mm. The difference between the maximum PTE at f_0 obtained from simulations and that measured experimentally is due to the presence of plastic fixing components used in the prototype. The obtained results highlight the strong influence of physical parameters on system performance, offering valuable insights for the design of compact and efficient wireless charging solutions. These combined factors partly explain the discrepancy observed between simulated and experimental PTE results and should be considered when the performance of the proposed WPT system is interpreted.

6. CONCLUSION

An investigation on the design, optimization, and implementation of the 4-coil MCR-WPT is proposed. The theoretical design method enabling reaching maximal PTE is elaborated. After expressing the S-parameters in terms of efficiency, 3-D full-wave CST simulations of PoC confirm that the performance was improved by the tuning process, reaching as high as 90.15% and the ratio $TD/D_{out} = 0.77$. Moreover, through coils optimization, it has been found that for each value of RD, there is an optimal distance TD that maximizes the efficiency, but for smaller TD, there are better results. The research work results enable us to state that increasing the number of coil turns enhances the PTE. Despite the validation of the 4-coil MCR-WPT design and optimization methodology, a prototype was fabricated with 3-D printing via a CAD tool, intended to operate at f_0. The maximal PTEs were identified at optimal values of physical distances RD and TD. However, it is found that the experimental results are less efficient than calculation and simulation due to the fabrication imperfections. For future work, this research could be useful to design an automatic maximum power tracker of the WPT system by varying the distance RD. Moreover, the proposed method can be extended to other coil geometries, offering additional flexibility for diverse applications. Future developments may also benefit from AI-based optimization techniques to enhance performance and enable automated design.

ACKNOWLEDGEMENT

This research work is supported by the Beijing Natural Science Foundation under Grant L233002.

REFERENCES

[1] Laha, A., A. Kalathy, M. Pahlevani, and P. Jain, "A comprehensive review on wireless power transfer systems for charging portable electronics," *Eng*, Vol. 4, No. 2, 1023–1057, 2023.

[2] Hui, S. Y., "Planar wireless charging technology for portable electronic products and Qi," *Proceedings of the IEEE*, Vol. 101, No. 6, 1290–1301, Jun. 2013.

[3] Philips, G. R., C. Clark, J. Wallace, C. Coopmans, Z. Pantic, and C. Bodine, "User-centred design, evaluation, and refinement of a wireless power wheelchair charging system," *Disability and Rehabilitation: Assistive Technology*, Vol. 17, No. 7, 815–827, 2022.

[4] Zhang, X., S. L. Ho, and W. N. Fu, "A hybrid optimal design strategy of wireless magnetic-resonant charger for deep brain stimulation devices," *IEEE Transactions on Magnetics*, Vol. 49, No. 5, 2145–2148, May 2013.

[5] Degen, C., "Inductive coupling for wireless power transfer and near-field communication," *EURASIP Journal on Wireless Communications and Networking*, Vol. 2021, No. 1, 121, May 2021.

[6] Wang, Y., Z. Sun, Y. Guan, and D. Xu, "Overview of megahertz wireless power transfer," *Proceedings of the IEEE*, Vol. 111, No. 5, 528–554, May 2023.

[7] Zhu, J.-Q., Y.-L. Ban, R.-M. Xu, and C. C. Mi, "An NFC-connected coupler using IPT-CPT-combined wireless charging for metal-cover smartphone applications," *IEEE Transactions on Power Electronics*, Vol. 36, No. 6, 6323–6338, Jun. 2021.

[8] Moon, S. and G.-W. Moon, "Wireless power transfer system with an asymmetric four-coil resonator for electric vehicle battery chargers," *IEEE Transactions on Power Electronics*, Vol. 31, No. 10, 6844–6854, Oct. 2016.

[9] Zhang, L., W. Tian, H. Ding, K. Lu, W. Hong, and R. Liu, "A hybrid magnetic couplers of wireless charging system for electric vehicles," *Progress In Electromagnetics Research C*, Vol. 101, 187–202, 2020.

[10] Cai, J., Y. Chen, A. D. Cheok, Y. Yan, and X. Zhang, "Overview of coupling coil design for magnetic coupled resonance wireless charging system of electric vehicles," *IEEE Transactions on Transportation Electrification*, Vol. 11, No. 4, 8903–8918, Aug. 2025.

[11] Li, S. and C. C. Mi, "Wireless power transfer for electric vehicle applications," *IEEE Journal of Emerging and Selected Topics in Power Electronics*, Vol. 3, No. 1, 4–17, Mar. 2015.

[12] Zhang, H., F. Lu, H. Hofmann, W. Liu, and C. C. Mi, "A four-plate compact capacitive coupler design and LCL-compensated topology for capacitive power transfer in electric vehicle charging application," *IEEE Transactions on Power Electronics*, Vol. 31, No. 12, 8541–8551, Dec. 2016.

[13] Dai, J. and D. C. Ludois, "A survey of wireless power transfer and a critical comparison of inductive and capacitive coupling for small gap applications," *IEEE Transactions on Power Electronics*, Vol. 30, No. 11, 6017–6029, Nov. 2015.

[14] Zhang, Y., S. Chen, X. Li, and Y. Tang, "Design methodology of free-positioning nonoverlapping wireless charging for consumer electronics based on antiparallel windings," *IEEE Transactions on Industrial Electronics*, Vol. 69, No. 1, 825–834, 2022.

[15] Zhong, W. X., X. Liu, and S. Y. R. Hui, "A novel single-layer winding array and receiver coil structure for contactless battery charging systems with free-positioning and localized charging features," *IEEE Transactions on Industrial Electronics*, Vol. 58, No. 9, 4136–4144, Sep. 2011.

[16] Covic, G. A. and J. T. Boys, "Modern trends in inductive power transfer for transportation applications," *IEEE Journal of Emerging and Selected Topics in Power Electronics*, Vol. 1, No. 1, 28–41, Mar. 2013.

[17] Adabi, R. N., K. Uehara, N. Shibata, and M. Inamori, "Investigation of data transmission for wireless power transfer system in seawater," in *2023 22nd International Symposium on Communications and Information Technologies (ISCIT)*, 399–402, Sydney, Australia, 2023.

[18] Sato, N., H. Kifune, and S. Komeda, "A coil layout of wireless power transfer systems based on multicoil arrangement for underwater vehicles," *Electrical Engineering in Japan*, Vol. 207, No. 2, 38–48, 2019.

[19] Yang, C., T. Wang, and Y. Chen, "Design and analysis of an omnidirectional and positioning tolerant AUV charging platform," *IET Power Electronics*, Vol. 12, No. 8, 2108–2117, 2019.

[20] Omata, S., K. Terada, and A. Kurokawa, "Design and analysis of coil sensors for position recognition in wireless charging," in *2025 15th International Conference on Power, Energy, and Electrical Engineering (CPEEE)*, 247–251, Fukuoka, Japan, 2025.

[21] Wang, M., L. Ren, W. Liu, Y. Shi, and Y. Niu, "Analysis and design of an efficient distance less-sensitive wireless power transfer system," *Progress In Electromagnetics Research C*, Vol. 106, 199–213, 2020.

[22] Nakamura, T., T. Hirata, E. Setiawan, and I. Hodaka, "A practical method for estimating mutual inductance in wireless power transmission system," *International Journal of Circuits, Systems and Signal Processing*, Vol. 16, 1027–1034, 2022.

[23] Kang, S. H. and C. W. Jung, "Magnetic resonant wireless power transfer with rearranged configurations," *Journal of Electromagnetic Engineering and Science*, Vol. 17, No. 2, 76–85, Apr. 2017.

[24] Truong, B. D., "Investigation on power optimization principles for series-configured resonant coupled wireless power transfer systems," *AEU — International Journal of Electronics and Communications*, Vol. 106, 67–81, 2019.

[25] Jabbari, A., C. Simovski, and M. S. M. Mollaei, "Tunable dual-band high-impedance coil for wireless power transfer applications," *IEEE Transactions on Antennas and Propagation*, Vol. 71, No. 12, 9467–9476, 2023.

[26] De Miranda, C. M., S. F. Pichorim, and P. J. Abatti, "On the impact of relay circuit losses in four-coil wireless power transfer systems," *International Journal of Circuit Theory and Applications*, Vol. 47, No. 12, 1922–1932, 2019.

[27] Chaimool, S., C. Rakluea, P. Akkaraekthalin, and Y. Zhao, "Effect of losses in printed rectangular coils for compact wireless power transfer systems," *Progress In Electromagnetics Research C*, Vol. 97, 177–188, 2019.

[28] Jabłoński, P., D. Kusiak, and T. Szczegielniak, "Analytical-numerical approach to the skin and proximity effect in lines with round parallel wires," *Energies*, Vol. 13, No. 24, 6716, 2020.

[29] Qiu, H., X. Zhang, J. Chen, M. Takamiya, and Y. Shi, "A 6.78-MHz coupling coefficient sensorless wireless power transfer system charging multiple receivers with efficiency maximization by adaptive magnetic field distributor IC," *IEEE Transactions on Circuits and Systems I: Regular Papers*, Vol. 71, No. 2, 974–983, 2024.

[30] Wang, T. and C. Yang, "Magnetic field optimization for high-positioning-tolerant wireless charging platforms," *Journal of Power Electronics*, Vol. 20, No. 1, 22–33, 2020.

[31] De Moraes, V. T. M., W. Kabbara, M. Bensetti, and T. Phulpin, "Modeling and optimization of a new magnetic coupler topology for DIPT systems," *IEEE Transactions on Magnetics*, Vol. 59, No. 5, 1–4, May 2023.

[32] Okamoto, Y., S. Wakao, and S. Sato, "Topology optimization based on regularized level-set function for solving 3-D nonlinear magnetic field system with spatial symmetric condition," *IEEE Transactions on Magnetics*, Vol. 52, No. 3, 1–4, Mar. 2016.

[33] Liu, T., J. Voigt, Z. Sun, A. Schnabel, Knappe-Grueneberg, I. Fan, and L. Li, "Two-step mirror model for the optimization of the magnetic field generated by coils inside magnetic shielding," in *2018 Conference on Precision Electromagnetic Measurements (CPEM 2018)*, 1–2, Paris, France, 2018.

[34] Matsumoto, H., W. Yoneyama, A. Hata, and Y. Sato, "Effective circuit configuration and control for coil-array wireless power transmitters," *IEEE Open Journal of the Industrial Electronics Society*, Vol. 4, 149–158, 2023.

[35] Huh, S., B. Park, S. Choi, Y. Shin, H. Kim, J. Kim, J. Park, D. Park, and S. Ahn, "Transmitter coils selection method for wireless power transfer system with multiple transmitter coils and single receiver coil," *IEEE Transactions on Power Electronics*, Vol. 38, No. 3, 4092–4109, 2023.

[36] Mirbozorgi, S. A., E. Maghsoudloo, H. Bahrami, M. Sawan, and B. Gosselin, "Multi-resonator arrays for smart wireless power distribution: Comparison with experimental assessment," *IET Power Electronics*, Vol. 13, No. 18, 4183–4193, 2020.

[37] Cao, Y. and J. A. A. Qahouq, "Evaluation of input power splitting wireless power transfer system with multiple transmitters for efficiency maximisation," *IET Power Electronics*, Vol. 12, No. 10, 2485–2492, 2019.

[38] Tan, S. Y., H. J. Lee, K. Y. Lau, and P. J. Ker, "Simulation of 4-coils magnetic resonance coupling for multiple receivers

wireless power transfer at various transmission distance," in *2018 IEEE Student Conference on Research and Development (SCOReD)*, 1–5, Selangor, Malaysia, Nov. 2018.

[39] Li, Z., Y. Lai, J. Yi, and J. Li, "A method of tracking optimum efficiency for four-coil wireless power transfer system," *Progress In Electromagnetics Research B*, Vol. 76, 125–140, 2017.

[40] Nair, V. V. and J. R. Choi, "An efficiency enhancement technique for a wireless power transmission system based on a multiple coil switching technique," *Energies*, Vol. 9, No. 3, 156, Mar. 2016.

[41] Kiani, M., U.-M. Jow, and M. Ghovanloo, "Design and optimization of a 3-coil inductive link for efficient wireless power transmission," *IEEE Transactions on Biomedical Circuits and Systems*, Vol. 5, No. 6, 579–591, Dec. 2011.

[42] Tan, S. Y. and H. J. Lee, "Critical review and simulation of mid-range wireless power transfer for electronic device," *Journal of Physics: Conference Series*, Vol. 1019, No. 1, 012002, 2018.

[43] Abduljaleel, H., S. Mutashar, and S. Gharghan, "Survey of near-field wireless communication and power transfer for biomedical implants," *Engineering and Technology Journal*, Vol. 42, No. 8, 1080–1103, 2024.

[44] Shevchenko, V., B. Pakhaliuk, O. Husev, O. Veligorskyi, D. Stepins, and R. Strzelecki, "Feasibility study GaN transistors application in the novel split-coils inductive power transfer system with T-type inverter," *Energies*, Vol. 13, No. 17, 4535, Sep. 2020.

[45] Xu, J., L. Gu, Z. Ye, S. Kargarrazi, and J. M. Rivas-Davila, "Cascode GaN/SiC: A wide-bandgap heterogenous power device for high-frequency applications," *IEEE Transactions on Power Electronics*, Vol. 35, No. 6, 6340–6349, Jun. 2020.

[46] Hussain, I. and D.-K. Woo, "Inductance calculation of single-layer planar spiral coil," *Electronics*, Vol. 11, No. 5, 750, 2022.

[47] Pacurar, C., V. Topa, C. Constantinescu, C. Munteanu, M. Gliga, S. Andreica, and A. Giurgiuman, "Adapting the formula for planar spiral inductors' inductance computation to the new oval geometric shape, ideal for designing wireless power transfer systems for smart devices," *Mathematics*, Vol. 13, No. 3, 348, Jan. 2025.

[48] Liu, X., C. Xia, and X. Yuan, "Study of the circular flat spiral coil structure effect on wireless power transfer system performance," *Energies*, Vol. 11, No. 11, 2875, Oct. 2018.

[49] Cruciani, S., T. Campi, F. Maradei, and M. Feliziani, "Numerical modeling of Litz wires based on discrete transpositions of strands and 2-D finite element analysis," *IEEE Transactions on Power Electronics*, Vol. 38, No. 5, 6710–6719, May 2023.

[50] Wu, B., X. Zhang, X. Liu, and C. He, "An analytical model for predicting the self-capacitance of multi-layer circular-section induction coils," *IEEE Transactions on Magnetics*, Vol. 54, No. 5, 1–7, May 2018.

[51] Özüpak, Y., "Analysis and experimental verification of efficiency parameters affecting inductively coupled wireless power transfer systems," *Heliyon*, Vol. 10, No. 5, e27420, 2024.